Editors' Suggestion

Observation of Symmetry-Protected Selection Rules in Periodically Driven Quantum Systems

Guoqing Wang (王国庆),[1,*] Changhao Li (李长昊),[1,*] and Paola Cappellaro[1,2,†]
[1]Research Laboratory of Electronics and Department of Nuclear Science and Engineering, Massachusetts Institute of Technology, Cambridge, Massachusetts 02139, USA
[2]Department of Physics, Massachusetts Institute of Technology, Cambridge, Massachusetts 02139, USA

(Received 25 May 2021; revised 9 August 2021; accepted 9 September 2021; published 29 September 2021)

Periodically driven (Floquet) quantum systems have recently been a focus of nonequilibrium physics by virtue of their rich dynamics. Time-periodic systems not only exhibit symmetries that resemble those in spatially periodic systems, but also display novel behavior that arises from symmetry breaking. Characterization of such dynamical symmetries is crucial, but often challenging due to limited driving strength and lack of an experimentally accessible characterization technique. Here, we show how to reveal dynamical symmetries, namely, parity, rotation, and particle-hole symmetries, by observing symmetry-induced Floquet selection rules. Notably, we exploit modulated driving to reach the strong light-matter coupling regime, and we introduce a protocol to experimentally extract the transition matrix elements between Floquet states from the system coherent evolution. By using nitrogen-vacancy centers in diamond as an experimental test bed, we execute our protocol to observe symmetry-protected dark states and dark bands, and coherent destruction of tunneling. Our work shows how one can exploit the quantum control toolkit to study dynamical symmetries that arise in the topological phases of strongly driven Floquet systems.

DOI: 10.1103/PhysRevLett.127.140604

Symmetries play an important role in determining system properties: they can lead to intriguing physical phenomena, such as topological phases [1–7], and universality classes [8]. As an example, different phases of topological insulators have been arranged into a periodic table [1]. Engineering novel quantum materials with desired symmetry properties [2–5] can be challenging. Time-periodic systems provide an alternative solution with increased versatility, even enabling novel dynamical phases that are absent in static systems [9–14], as the periodic driving can force the system towards topological phases [15–17]. These dynamical time symmetries are described by Floquet theory [6], in analogy to the description of spatial symmetries by Bloch theory.

A hallmark of symmetries is the presence of induced selection rules. Selection rules of transitions between Floquet states have recently been analyzed theoretically [18], but their experimental observation remains challenging. First, although strong light-matter coupling is required to generate high-order Floquet bands, this regime is difficult to reach in practice due to the finite strength of the driving fields. Second, observing the selection rules requires an experimental toolkit that enables an extraction of transition elements between Floquet states. In this Letter, we tackle both challenges and provide a feasible solution by combining modulated driving with the observation of the subsequent quantum coherent dynamics, to experimentally detect symmetry-induced selection rules—and their breaking.

Recent years have witnessed a rapid development of exquisite quantum control techniques that can enable engineered driving beyond hardware limitations [19]. For example, concatenated continuous driving (CCD), originally introduced to counteract driving inhomogeneities in dynamical decoupling [20–22], has recently been shown to allow one to reach the strong-coupling regime and uncover phenomena such as high-order Mollow triplets [23] that would be "invisible" in simple driving protocols. Here we exploit modulated driving not only to achieve an effective strong-coupling regime even with limited driving strength, but also to engineer driving transitions (such as double-quantum transitions) that would otherwise not be directly accessible. To extract transition elements between Floquet states, we further develop a protocol based on monitoring the coherent state evolution by projective measurements, which enacts a mapping of the dynamical dipole matrix elements describing Floquet band transitions to measurable Rabi oscillation amplitudes. We take advantage of the controllability and long coherence times achieved in qubit-like systems [24–26], avoiding the need for dissipation and for "pump-probe" methods traditional in atomic and optical physics. Our method, also applicable to general N-level quantum systems, is thus convenient in many modern quantum platforms.

By exploiting these technical advances, we are able to experimentally study parity and particle-hole symmetries by monitoring the evolution of two levels of a nitrogen-vacancy (NV) center in diamond, under modulated driving.

Our experiments reveal the emergence of dark states and dark bands and their vanishing once the corresponding symmetries are broken—as well as coherent destruction of tunneling [27–30]. We further show that modulated driving can engineer a rotationally symmetric Hamiltonian over the NV center three levels, further indicating that our methods are broadly applicable, and exemplify an important step toward exploring topological phases that arise in Floquet systems [10].

Methods.—Spatially periodic Hamiltonians in solid-state physics can be analyzed by Bloch theory, which predicts a periodic structure in reciprocal space. Likewise, the dynamics of a periodically driven Hamiltonian $\mathcal{H}(t) = \mathcal{H}(t+T)$ is solved by Floquet theory, yielding a series of equidistant energy bands (manifolds) $\lambda^\mu + n\omega_m$ ($n \in Z$) with Floquet eigenenergies λ^μ and frequencies $\omega_m = 2\pi/T$ [6,31]. The time-dependent Schrödinger equation is indeed equivalent to the eigenvalue problem for a time-independent Floquet matrix $[\mathcal{H}(t) - i(\partial/\partial t)]|\Phi^\mu(t)\rangle = \lambda^\mu|\Phi^\mu(t)\rangle$. The Floquet eigenstates $|\Phi^\mu(t)\rangle$ have the same period as the Hamiltonian and can be decomposed into Fourier series as $|\Phi^\mu(t)\rangle = \sum_{n=-\infty}^{+\infty} e^{-in\omega_m t}|\Phi_n^\mu\rangle$ [31]. The evolved state is then a superposition of Floquet eigenstates,

$$|\Psi(t)\rangle = \sum_\mu c^\mu e^{-it\lambda^\mu}|\Phi^\mu(t)\rangle = \sum_{\mu,n} c^\mu|\Phi_n^\mu\rangle e^{-it(n\omega_m+\lambda^\mu)}, \quad (1)$$

with the coefficients c^μ set by initial conditions at $t = 0$.

Consider a time-independent symmetry operator $\hat{\mathcal{S}}$ (rotation, parity, particle-hole, etc.) satisfying

$$\hat{\mathcal{S}}\left[\mathcal{H}(\beta_{\mathcal{S}}t + t_{\mathcal{S}}) - i\frac{d}{dt}\right]\hat{\mathcal{S}}^{-1} = \alpha_{\mathcal{S}}\left[\mathcal{H}(t) - i\frac{d}{dt}\right], \quad (2)$$

where $\{\alpha_{\mathcal{S}}, \beta_{\mathcal{S}}\} \in \{1, -1\}$ and $t_{\mathcal{S}}$ define the detailed parameters of the symmetry. Then the Floquet eigenstates also have the same symmetry $|\Phi^{\mu'}(t)\rangle = \pi_\mu^{\mathcal{S}}\hat{\mathcal{S}}|\Phi^\mu(\beta_{\mathcal{S}}t + t_{\mathcal{S}})\rangle$, with $|\pi_\mu| = 1$, as derived in Ref. [18]. These symmetries can be probed by evaluating the susceptibility, e.g., in light scattering experiments of a probe field V, in analogy with "pump-probe" schemes common in atomic and optical physics. The susceptibility depends on the dynamical dipole matrix elements associated with the probing operator V

$$V_{\mu,\nu}^{(n)} = \frac{1}{T}\int_0^T \langle\Phi^\mu(t)|V|\Phi^\nu(t)\rangle e^{-in\omega_m t}dt, \quad (3)$$

where n denotes the energy band order. When $\hat{\mathcal{S}}^\dagger V\hat{\mathcal{S}} = \alpha_V V$, the dynamical symmetry gives rise to symmetry-protected selection rules, including symmetry-protected dark states (spDSs) for $V_{\mu,\nu}^{(n)} = 0$, symmetry-protected dark bands (spDBs) for vanishing susceptibility of complete bands, and symmetry-induced transparency (siT) due to the destructive interference between nonzero elements [18,32].

Rather than measuring the susceptibility in a pump-probe experiment [18], here we establish a general experimental method to directly measure the dipole operator V. Specifically, we draw a correspondence between the dipole matrix elements, typical of light scattering experiments, and measurable Rabi oscillation amplitudes arising in the context of coherent state evolution. We show that in a coherent system, the amplitudes of the Fourier components of $\langle V(t)\rangle$ display the desired properties (spDBs, spDSs, siT, etc.) associated with dipole matrix elements $V_{\mu,\nu}^{(n)}$.

We consider a generic N-level quantum system and introduce the spectral decomposition $V = \sum_k \mathcal{V}_k|k\rangle\langle k|$, such that the dipole matrix elements in Eq. (3) can be calculated as

$$V_{\mu,\nu}^{(n)} = \mathcal{V}_k\sum_p \langle\Phi_p^\mu|k\rangle\langle k|\Phi_{p-n}^\nu\rangle. \quad (4)$$

From Eqs. (1), (4) the expectation value of $V(t)$ is then

$$\langle V\rangle = \langle\Psi(t)|V|\Psi(t)\rangle = \sum_{\mu,\nu,n} c^{\mu*}c^\nu e^{i(\lambda^\mu-\lambda^\nu)t}e^{in\omega_m t}V_{\mu,\nu}^{(n)}. \quad (5)$$

By considering the Fourier decomposition of $\langle V\rangle$,

$$\langle V\rangle = \sum_{\mu,\nu,n}|A_{\mu,\nu}^{(n)}|\cos(\omega_{\mu,\nu}^{(n)}t + \phi_{\mu,\nu}^{(n)}), \quad (6)$$

with frequencies $\omega_{\mu,\nu}^{(n)} = n\omega_m + (\lambda^\mu - \lambda^\nu)$, we find that the Fourier amplitudes

$$A_{\mu,\nu}^{(n)} = |A_{\mu,\nu}^{(n)}|\exp(i\phi_{\mu,\nu}^{(n)}) = 2c^{\mu*}c^\nu V_{\mu,\nu}^{(n)} \quad (7)$$

can be used to extract the dipole matrix elements.

Since in general it might be difficult to directly measure the operator V, one can rely on system preparation and readout to separately monitor the overlap of the state with the eigenstates of V, i.e., $P_{|k\rangle}(t) = |\langle k|\Psi(t)\rangle|^2$. We can then analyze the "*weighted Rabi*" oscillations

$$P(t) = \sum_k \frac{\mathcal{V}_k}{\mathcal{V}}P_{|k\rangle}(t) \equiv \frac{\langle V\rangle}{\mathcal{V}}, \quad \text{with} \quad \mathcal{V} = \sum_k|\mathcal{V}_k|. \quad (8)$$

The weighted Rabi oscillations can then be decomposed into frequency components with amplitudes $a_{\mu,\nu}^{(n)} = A_{\mu,\nu}^{(n)}/\mathcal{V}$, which can be used to investigate symmetry properties. For example, consider a two-level system (TLS). The probing operator V is then a combination of Pauli operators σ_j with eigenvectors $|0_j\rangle$, $|1_j\rangle$ and normalized eigenvalues ± 1. The weighted Rabi oscillations have the form $P(t) = (1/2)[P_{|0_j\rangle}(t) - P_{|1_j\rangle}(t)]$ which can be simplified to the typical Rabi oscillations $P(t) + 1/2 = P_{|0_j\rangle}(t)$, thus clarifying

the connection of our protocol with typical Rabi measurements.

In addition to using control of the readout state to measure $P_{|k\rangle}$, we can also control the initial state to extract information about selected dipole matrix elements, by appropriately choosing the coefficients c^{μ}.

When $\mu = \nu$, all bands under the same order (n) are degenerate with frequency $n\omega_m$ (*centerbands*), and the observed Rabi component is their coherent interference with an amplitude $a_0^{(n)} = 2\sum_{\mu} |c^{\mu}|^2 V_{\mu,\mu}^{(n)}/\mathcal{V}$. Each band $V_{\mu,\mu}^{(n)}$ can also be observed individually by setting the initial condition $|c^{\mu}| = 1$ (this tuning is known as *quantum mode control*) [23].

When $\mu \neq \nu$, the off-diagonal dipole matrix elements $V_{\mu,\nu}^{(n)}$ can be mapped to the Rabi amplitudes $a_{\mu,\nu}^{(n)}$ corresponding to the bands $n\omega_m + (\lambda^{\mu} - \lambda^{\nu})$ (*sidebands*). At the degeneracy points (e.g., $\lambda^{\mu} = \lambda^{\nu}$), different sidebands interfere with each other, inducing phenomena such as the siT, or more generally the Landau-Zener-Stückelberg interferometry [42,43] and coherence destruction of tunneling (CDT) [27–30].

Results.—To demonstrate the power of combining modulated driving with weighted Rabi measurements we characterize symmetries arising in two- and three-level systems, experimentally realized using NV centers.

NV centers in diamond are atomlike solid-state defects with a triplet ground state labelled by $|m_s = 0, \pm 1\rangle$ with long-coherence time that enables their applications in quantum information science, including quantum sensing [44–48] and quantum control [15,22]. To truncate the 3-level NV center to an effective TLS, we break the $|m_s = \pm 1\rangle$ degeneracy by applying an external magnetic field with strength 239 G, and selectively use the two ground states $|m_s = 0\rangle$ and $|m_s = -1\rangle$ as logical $|0\rangle$ and $|1\rangle$ [22,23,49]. We simultaneously address an ensemble of noninteracting NV centers ($\sim 10^{10}$ qubits) to increase the signal-to-noise ratio. An arbitrary waveform generator (WX1284C) is used to generate the desired waveform for Hamiltonian engineering.

To engineer strong driving on the NV centers, we rely on the phase-modulated CCD technique [50], which has been applied previously to approach the strong-coupling regime even with limited driving fields [20–22]. As shown in Fig. 1(a), we apply a phase-modulated waveform

$$\mathcal{H} = \frac{\omega_0}{2}\sigma_z + \Omega \cos\left(\omega_0 t + \frac{2\epsilon_m}{\omega_m}\cos(\omega_m t + \phi)\right)\sigma_x, \tag{9}$$

where $\omega_0 = (2\pi)2.20$ GHz is the qubit frequency, Ω the microwave driving strength, and ϵ_m, ω_m, ϕ are modulation parameters. In the interaction picture defined by $U = \exp\{-i((\omega_0 t/2)\sigma_z + \epsilon_m[\cos(\omega_m t + \phi)/\omega_m]\sigma_z)\}$, the Hamiltonian $\mathcal{H}_I = U^{\dagger}\mathcal{H}U - U^{\dagger}i(d/dt)U$ is

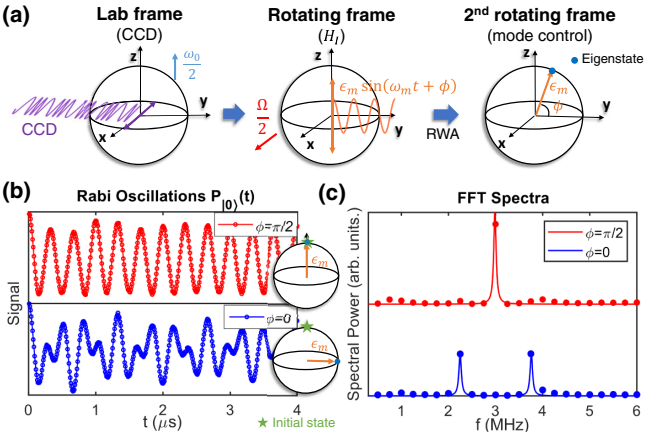

FIG. 1. (a) Sketch of the CCD technique for a TLS. (b) Rabi oscillations of $|0\rangle$ state under different modulation phases ϕ with other parameters $(\Omega, \omega_m, \epsilon_m) = (2\pi)(3, 3, 0.75)$ MHz. (c) The FFT spectra of Rabi oscillations in (b).

$$\mathcal{H}_I = \frac{\Omega}{2}\sigma_x + \epsilon_m \sin(\omega_m t + \phi)\sigma_z. \tag{10}$$

We thus obtain a time-periodic Hamiltonian $\mathcal{H}_I$ with $T = 2\pi/\omega_m$, where Ω and ϵ_m behave as the static and driving fields, respectively, and their relative strength can be easily tuned to approach the strong coupling regime, without hardware limitations.

The periodic Hamiltonian $\mathcal{H}_I(t)$ in Eq. (10) has two nontrivial Floquet eigenenergies $\lambda^{\pm}$ and the transitions in the complete Floquet energy structure form Mollow triplets $\omega_i^{(n)} = n\omega_m + i(\lambda^{+} - \lambda^{-})$. Here $i = 0, \pm 1$ correspond to the centerbands and sidebands, respectively. These transitions can be probed either through conventional pump-probe spectroscopy, such as spontaneous emission [51], or via projective Rabi measurements in the context of coherent state evolution [23,33,52], where the Rabi amplitudes can be exactly mapped to the dipole matrix element (Table I). Under a weak-coupling regime, the Floquet eigenenergies and eigenstates can also be analytically obtained in a second rotating frame as shown in Fig. 1(a). Figures 1(b),1(c) show instances of the Rabi measurement in time and frequency domains where different Mollow bands are separately measured under different initial conditions.

In the following, we experimentally evaluate the dynamical symmetries of the qubit Hamiltonian $\mathcal{H}_I$, and study the associated spDSs, spDBs, and siT through the intensities of the Floquet state transitions, which are extracted from Rabi oscillations.

The first dynamical symmetry is a twofold rotation or parity symmetry defined by $\hat{R} = \sigma_x$, which satisfies $\hat{R}\mathcal{H}_I(t + T/2)\hat{R}^{\dagger} = \mathcal{H}_I(t)$. The selection rules are then given by $V_{\mu,\nu}^{(n)} \propto [1 + e^{i\pi(m_{\mu} - m_{\nu}) - i\pi n}\alpha_V^{(R)}]$, where $\mu \in \{+, -\}$, $m_{\mu} \in \{0, 1\}$, and the constant $\alpha_V^{(R)}$ satisfies $\hat{R}^{\dagger}V\hat{R} = \alpha_V^{(R)}V$.

TABLE I. Correspondence between the Rabi amplitudes $a_i^{(n)}$ and dipole matrix element $V_{\mu,\nu}^{(n)}$ for a TLS. Note that $\Phi_{p,0_j}^{\mu} = \langle 0_j | \Phi_p^{\mu} \rangle$, and listed cases do not include $i = n = 0$ [23,32].

Bands$_{\{i,n\}}$	Rabi amplitudes $a_{\mu,\nu}^{(n)}$	Expressed in $V_{\mu,\nu}^{(n)}$
$\{0, n\}$	$2\sum_{\pm} \lvert c^{\pm}\rvert^2 \sum_k \Phi_{k+n,0_j}^{\pm *} \Phi_{k,0_j}^{\pm}$	$\lvert c^{+}\rvert^2 V_{+,+}^{(n)} + \lvert c^{-}\rvert^2 V_{-,-}^{(n)}$
$\{-1, n\}$	$2\sum_k c^{+} c^{-*} \Phi_{k,0_j}^{+} \Phi_{k+n,0_j}^{-*}$	$c^{+} c^{-*} V_{-,+}^{(n)}$
$\{+1, n\}$	$2\sum_k c^{+*} c^{-} \Phi_{k+n,0_j}^{+*} \Phi_{k,0_j}^{-}$	$c^{+*} c^{-} V_{+,-}^{(n)}$

For observation operators that anticommute with the symmetry operator ($V = \sigma_y, \sigma_z$), the Mollow center bands with even orders and sidebands with odd orders vanish. The opposite holds for the commuting observation operator ($V = \sigma_x$). As a result, a series of spDSs and spDBs are predicted by the parity symmetry.

To experimentally observe these selection rules, we measure the Rabi oscillations under different modulation strengths $2\epsilon_m/\omega_m$ and plot their Fourier spectrum. In Figs. 2(a),2(b), the 1st, 3rd, 5th Mollow sidebands, and 2nd, 4th Mollow centerbands have vanishing intensities, as indicated by dashed lines and labels where nonzero transition amplitudes would otherwise have been expected. In Figs. 2(c),2(d), the opposite behavior is observed. These results validate the theoretical analysis. Note that some unexpected bands [e.g., odd order centerbands in the range of $2.5 < 2\epsilon_m/\omega_m < 5$ in Figs. 2(c),2(d)] are still visible, albeit with small intensities. We attribute their occurrence to experimental imperfections such as inhomogeneities that introduce a detuning term in the Hamiltonian $\mathcal{H}_I$ [22,32].

The second symmetry is a particle-hole symmetry defined by $\hat{P}_1 = \sigma_z$, which satisfies $\hat{P}_1 \mathcal{H}_I(t + T/2)\hat{P}_1^{\dagger} = -\mathcal{H}_I(t)$. The selection rules are then given by $V_{\mu,\nu}^{(n)} = \alpha_V^{(P_1)} e^{i\pi n} V_{\nu',\mu'}^{(n)}$, where $\alpha_V^{(P_1)}$ satisfies $\hat{P}_1^{\dagger} V \hat{P}_1 = \alpha_V^{(P_1)} V^*$ [53]. For sidebands, the selection rules are consistent with the parity symmetry predictions as observed in Figs. 2(a)–2(d). For centerbands, destructive interference is induced when $\alpha_V^{(P_1)} e^{i\pi n} = -1$ and the initial state is an equal superposition of two eigenstates such that $V_{+,+}^{(n)} + V_{-,-}^{(n)} = 0$. This property gives rise to vanishing centerbands in the *quantum mode control* as shown in Fig. 1(c) and Ref. [23]. For a modulation phase $\phi = 0$, the Floquet eigenstates are in the $x - y$ plane of the Bloch sphere such that $\lvert c^{\pm}\rvert^2 = 1/2$ for the initial state $\lvert 0\rangle$, and the destructive interference transpires in the odd (even) centerband when $V = \sigma_z$ ($V = \sigma_x$). Combining with the parity symmetry that makes the opposite orders of centerband vanish, all centerbands vanish under $\phi = 0$ as observed in Figs. 2(a),2(c). Instead, under the modulation phase

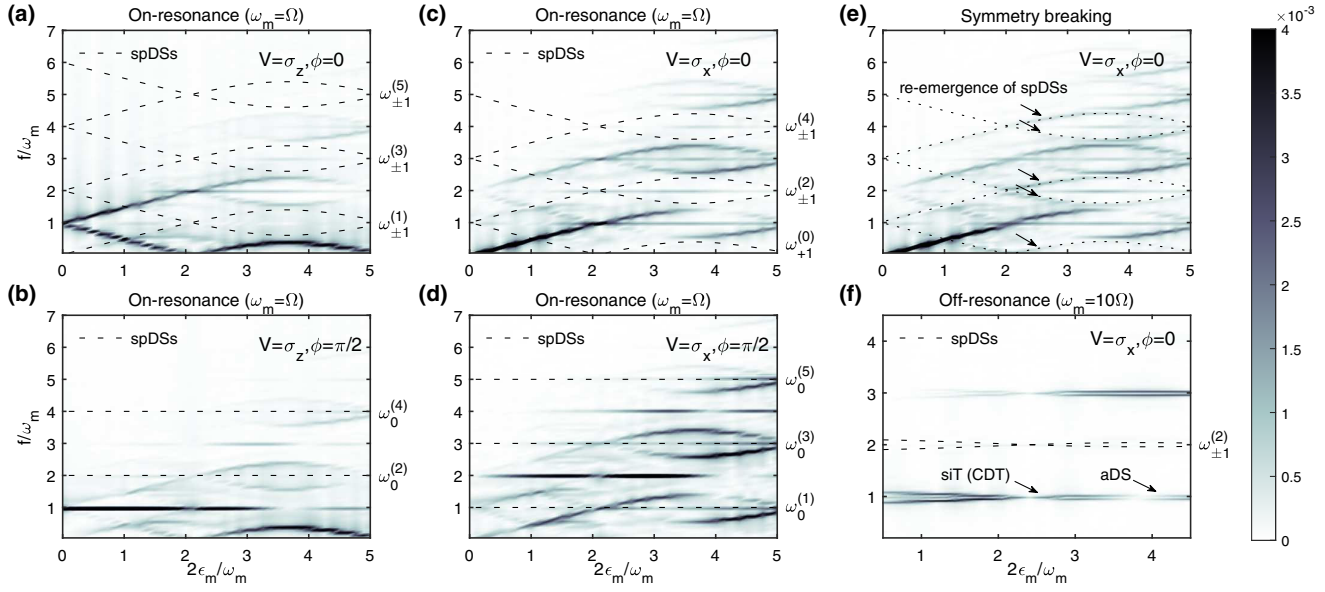

FIG. 2. Experimental observation of spDSs, spDBs, and siT. (a)–(d) Observation of spDSs, spDBs under resonant modulation $\omega_m = \Omega = (2\pi)3$ MHz. The initial state is $\lvert 0\rangle$, and we measure generalized Rabi oscillations $P_{\lvert 0\rangle}(t)$ or $P_{\lvert +\rangle}(t)$ under different modulation strength $2\epsilon_m/\omega_m$, from 0 to 4 μs with 401 sampling points (see Fig. 1.) The plots are the Fourier spectrum of the Rabi measurements for specified modulation phases ϕ and probe operator V. In (a) the odd sidebands vanish (spDSs, marked by dashed lines and labels). Similarly, we observe vanishing even (b) and odd (d) centerbands. The even sidebands vanish in (c), but they reemerge in (e) (arrows and dotted lines), due to symmetry breaking induced by adding a perturbation, $\mathcal{H}' = 0.2\epsilon_m \sin(2\omega_m t)\sigma_z$ to the periodic Hamiltonian. (f) Observations of siT, spDSs, spDBs and accidental dark states (aDS) under off-resonant modulation ω_m, $10\Omega = (2\pi)15$ MHz (labels indicate the revealing features). Rabi oscillations $P_{\lvert +\rangle}(t)$ of an initial state $\lvert 0\rangle$ are measured from 0 to 2 μs with 401 sampling points.

$\phi = \pi/2$, the Floquet eigenstates are in the $x-z$ plane and the condition $|c^{\pm}|^2 = 1/2$ is not always satisfied. The symmetry-allowed centerbands appear as shown in Figs. 2(b),2(d) and vanish at $2\epsilon_m/\omega_m \approx 4$, where $|c^{\pm}|^2 = 1/2$ is accidentally satisfied.

To further demonstrate the symmetry-protected selection rules, we break both the parity and particle-hole symmetries by introducing an additional term $0.2\epsilon_m \sin(2\omega_m t)\sigma_z$ in the Hamiltonian $\mathcal{H}_I$, and measure the Rabi spectrum in Fig. 2(e), where we see the emergence of all sidebands [odd allowed sidebands as in Fig. 2(c) and symmetry-breaking even sidebands.]

Another type of destructive interference, siT, is observable when sidebands interfere destructively at degeneracy points, which requires two discrete particle-hole symmetries in the system. In the strong coupling and far off-resonance regime ($\Omega \ll \epsilon_m$, ω_m), an additional particle-hole symmetry $\hat{P}_2 = I$ arises such that $I\mathcal{H}_I(t+T/2)I = -\mathcal{H}_I(t)$, which results in a relation between two sidebands $V^{(n)}_{+,-} = \alpha_V^{(P_1^*)} e^{i\pi n} V^{(n)}_{-,+}$ with $\alpha_V^{(P_1^*)}$ given by $\alpha_V^{(P_1^*)} V = \hat{P}_1{}^{\dagger *} V \hat{P}_1{}^{*}$. Under the initial condition $c^+ c^{-*} = c^{+*} c^-$, the siT happens when $\alpha_V^{(P_1^*)} e^{i\pi n} = -1$, and the qubit evolution is suppressed in the direction of the driving field (the CDT effect, which has been observed before both numerically [29] and experimentally [30].) In Fig. 2(f), we engineer a strong-coupling Hamiltonian and measure the Rabi spectrum. The siT is observed when two sidebands are degenerate at $2\epsilon_m/\omega_m = 2.4048$ (see Supplemental Material for a constructive interference [32]). In addition, spDSs are also observed as in Fig. 2(c).

In order to demonstrate that our technique can be extended beyond TLSs, we show how to use the 3 levels associated with the spin-1 of NV centers to explore a threefold rotation symmetry. We use modulated driving to both reach the strong driving regime and to engineer the double quantum (DQ) transition ($|m_S = -1\rangle \leftrightarrow |m_S = +1\rangle$) in the rotating frame. Indeed, the DQ transition cannot be directly generated by microwave driving (although it could be achieved by mechanical oscillations 54,55]].) Here we overcome this limitation by simultaneously applying two modulated driving on the single quantum transitions ($|m_S = 0\rangle \leftrightarrow |m_S = \pm 1\rangle$), leading to the rotating-frame Hamiltonian [32]

$$\mathcal{H}_I^3(t) = J[\cos(\omega_m t)|-1\rangle\langle+1| + \cos(\omega_m t + 2\pi/3)|+1\rangle\langle 0| + \cos(\omega_m t + 4\pi/3)|-1\rangle\langle 0| + \text{H.c.}] \tag{11}$$

with a threefold rotation symmetry $\hat{R}\mathcal{H}_I^3(t+T/3)\hat{R}^\dagger = \mathcal{H}_I(t)$, where the rotation $\hat{R} = |-1\rangle\langle 0| + |0\rangle\langle+1| + |+1\rangle\langle -1|$. We find symmetry-protected selections rules by evaluating the Floquet eigenstates and the observation operator [32]. In Fig. 3, we simulate the Fourier spectrum of the weighted Rabi signal for the probe operator $V = |0\rangle\langle+1| + |0\rangle\langle-1| + |+1\rangle\langle-1| + \text{H.c.}$, which clearly displays the expected spDSs, protected by the threefold rotation symmetry.

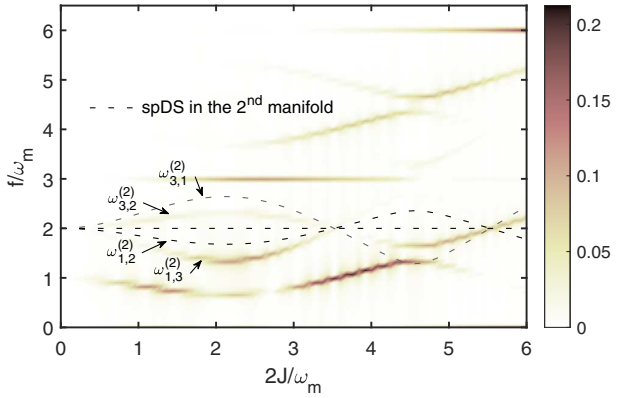

FIG. 3. Simulation of spDSs and spDBs in a three-level system (vanishing intensities marked by the dashed lines). The initial state is $(1/\sqrt{3})(|e_1\rangle + |e_2\rangle + |e_3\rangle)$ where $|e_{1,2,3}\rangle$ are eigenstates of V, such that evolution mode involves all bands. The weighted Rabi $P(t) = (1/4)[2P_{|e_1\rangle}(t) - P_{|e_2\rangle}(t) - P_{|e_3\rangle}(t)]$ is simulated from 0 to 40 μs with 5001 sampling points and the modulation frequency is 0.3 MHz.

Discussions and conclusion.—By combining modulated driving and detection via Rabi oscillations, we are able to experimentally observe selection rules protected by dynamical symmetries in a periodically driven solid-state system. The modulated driving scheme is instrumental to reach the strong light-matter coupling regime used to reveal high-order Floquet bands; it also introduces additional flexibility in quantum control, enabling one to engineer transitions forbidden in the unmodulated frame and reveal details of the dynamics (e.g., Mollow triplets) via mode control. Direct measurement of the dipolar transition operator V, or indirectly via weighted Rabi oscillations is a more efficient strategy than previous pump-probe methods in the highly coherent quantum systems that can now be routinely engineered. In virtue of these techniques, we characterized the time-domain parity and particle-hole symmetries as well as the CDT effect in the engineered system. In the context of quantum control, the dynamical symmetries studied here have applications in inducing selections rules for higher harmonic generation and driving quantum synchronization [56–59].

While we showed simulations and experiments for two- and three-level systems, the experimental techniques we introduced can be generalized to many-body (N-level) systems in a broad set of platforms beyond spins, such as cold atoms and superconducting circuits.

When combined with spatial symmetries, dynamical symmetries characterized in this work can lead to novel Floquet topological phases such as Floquet topological insulators and superconductors [10]. The breaking of these dynamical symmetries might lead to intriguing dynamical phase transitions. Furthermore, by engineering of the dissipation such as tuning the decoherence rate of the

system, the work here paves the way towards further exploration of non-Hermitian Floquet Hamiltonians.

This work was in part supported by ARO Grant No. W911NF-11-1-0400 and NSF Grants No. PHY1734011 and No. EECS1702716. We thank Pai Peng for fruitful discussions and Thanh Nguyen for manuscript revision.

*These authors contributed equally to this work.
†pcappell@mit.edu

[1] A. Kitaev, AIP Conf. Proc. **1134**, 22 (2009).
[2] M. Angeli and A. H. MacDonald, Proc. Natl. Acad. Sci. U.S.A. **118**, e2021826118 (2021).
[3] Y. Cao, V. Fatemi, S. Fang, K. Watanabe, T. Taniguchi, E. Kaxiras, and P. Jarillo-Herrero, Nature (London) **556**, 43 (2018).
[4] K. L. Seyler, P. Rivera, H. Yu, N. P. Wilson, E. L. Ray, D. G. Mandrus, J. Yan, W. Yao, and X. Xu, Nature (London) **567**, 66 (2019).
[5] K. Tran, G. Moody, F. Wu, X. Lu, J. Choi, K. Kim, A. Rai, D. A. Sanchez, J. Quan, A. Singh, J. Embley, A. Zepeda, M. Campbell, T. Autry, T. Taniguchi, K. Watanabe, N. Lu, S. K. Banerjee, K. L. Silverman, S. Kim, E. Tutuc, L. Yang, A. H. MacDonald, and X. Li, Nature (London) **567**, 71 (2019).
[6] J. H. Shirley, Phys. Rev. **138**, B979 (1965).
[7] X.-L. Yu, W. Ji, L. Zhang, Y. Wang, J. Wu, and X.-J. Liu, PRX Quantum **2**, 020320 (2021).
[8] G. Ódor, Rev. Mod. Phys. **76**, 663 (2004).
[9] A. Eckardt, Rev. Mod. Phys. **89**, 011004 (2017).
[10] R. Roy and F. Harper, Phys. Rev. B **96**, 155118 (2017).
[11] Y. Peng and G. Refael, Phys. Rev. Lett. **123**, 016806 (2019).
[12] K. Wintersperger, C. Braun, F. N. Ünal, A. Eckardt, M. D. Liberto, N. Goldman, I. Bloch, and M. Aidelsburger, Nat. Phys. **16**, 1058 (2020).
[13] P. Peng, C. Yin, X. Huang, C. Ramanathan, and P. Cappellaro, Nat. Phys. **17**, 444 (2021).
[14] C. Yin, P. Peng, X. Huang, C. Ramanathan, and P. Cappellaro, Phys. Rev. B **103**, 054305 (2021).
[15] M. C. Rechtsman, J. M. Zeuner, Y. Plotnik, Y. Lumer, D. Podolsky, F. Dreisow, S. Nolte, M. Segev, and A. Szameit, Nature (London) **496**, 196 (2013).
[16] G. Jotzu, M. Messer, R. Desbuquois, M. Lebrat, T. Uehlinger, D. Greif, and T. Esslinger, Nature (London) **515**, 237 (2014).
[17] K. Jiménez-García, L. J. LeBlanc, R. A. Williams, M. C. Beeler, C. Qu, M. Gong, C. Zhang, and I. B. Spielman, Phys. Rev. Lett. **114**, 125301 (2015).
[18] G. Engelhardt and J. Cao, Phys. Rev. Lett. **126**, 090601 (2021).
[19] A. Ajoy, Y.-X. Liu, K. Saha, L. Marseglia, J.-C. Jaskula, U. Bissbort, and P. Cappellaro, Proc. Natl. Acad. Sci. U.S.A. **114**, 2149 (2017).
[20] J.-M. Cai, B. Naydenov, R. Pfeiffer, L. P. McGuinness, K. D. Jahnke, F. Jelezko, M. B. Plenio, and A. Retzker, New J. Phys. **14**, 113023 (2012).
[21] D. Farfurnik, N. Aharon, I. Cohen, Y. Hovav, A. Retzker, and N. Bar-Gill, Phys. Rev. A **96**, 013850 (2017).
[22] G. Wang, Y.-X. Liu, and P. Cappellaro, New J. Phys. **22**, 123045 (2020).
[23] G. Wang, Y.-X. Liu, and P. Cappellaro, Phys. Rev. A **103**, 022415 (2021).
[24] E. Bauch, C. A. Hart, J. M. Schloss, M. J. Turner, J. F. Barry, P. Kehayias, S. Singh, and R. L. Walsworth, Phys. Rev. X **8**, 031025 (2018).
[25] M. Zhong, M. P. Hedges, R. L. Ahlefeldt, J. G. Bartholomew, S. E. Beavan, S. M. Wittig, J. J. Longdell, and M. J. Sellars, Nature (London) **517**, 177 (2015).
[26] S. Ebadi, T. T. Wang, H. Levine, A. Keesling, G. Semeghini, A. Omran, D. Bluvstein, R. Samajdar, H. Pichler, W. W. Ho, S. Choi, S. Sachdev, M. Greiner, V. Vuletić, and M. D. Lukin, Nature (London) **595**, 227 (2021).
[27] F. Grossmann, T. Dittrich, P. Jung, and P. Hänggi, Phys. Rev. Lett. **67**, 516 (1991).
[28] F. Grossmann, T. Dittrich, P. Jung, and P. Hänggi, J. Stat. Phys. **70**, 229 (1993).
[29] Z. Lü and H. Zheng, Phys. Rev. A **86**, 023831 (2012).
[30] J. Zhou, P. Huang, Q. Zhang, Z. Wang, T. Tan, X. Xu, F. Shi, X. Rong, S. Ashhab, and J. Du, Phys. Rev. Lett. **112**, 010503 (2014).
[31] M. Leskes, P. Madhu, and S. Vega, Prog. Nucl. Magn. Reson. Spectrosc. **57**, 345 (2010).
[32] See Supplemental Material at http://link.aps.org/supplemental/10.1103/PhysRevLett.127.140604 for details, which includes Refs. [18,20–23,31,33–41].
[33] S. Rohr, E. Dupont-Ferrier, B. Pigeau, P. Verlot, V. Jacques, and O. Arcizet, Phys. Rev. Lett. **112**, 010502 (2014).
[34] N. Khaneja, A. Dubey, and H. S. Atreya, J. Magn. Reson. **265**, 117 (2016).
[35] A. Saiko, R. Fedaruk, and S. Markevich, J. Magn. Reson. **290**, 60 (2018).
[36] I. Cohen, N. Aharon, and A. Retzker, Fortschr. Phys. **65**, 1600071 (2017).
[37] K. J. Layton, B. Tahayori, I. M. Mareels, P. M. Farrell, and L. A. Johnston, J. Magn. Reson. **242**, 136 (2014).
[38] A. P. Saiko, R. Fedaruk, and S. A. Markevich, J. Magn. Reson. **259**, 47 (2015).
[39] J. Teissier, A. Barfuss, and P. Maletinsky, J. Opt. **19**, 044003 (2017).
[40] S. Bertaina, H. Vezin, H. De Raedt, and I. Chiorescu, Sci. Rep. **10**, 21643 (2020).
[41] Q.-Y. Cao, P.-C. Yang, M.-S. Gong, M. Yu, A. Retzker, M. B. Plenio, C. Müller, N. Tomek, B. Naydenov, L. McGuinness, F. Jelezko, and J.-M. Cai, Phys. Rev. Applied **13**, 024021 (2020).
[42] S. Shevchenko, S. Ashhab, and F. Nori, Phys. Rep. **492**, 1 (2010).
[43] P. Huang, J. Zhou, F. Fang, X. Kong, X. Xu, C. Ju, and J. Du, Phys. Rev. X **1**, 011003 (2011).
[44] C. L. Degen, F. Reinhard, and P. Cappellaro, Rev. Mod. Phys. **89**, 035002 (2017).
[45] R. Schirhagl, K. Chang, M. Loretz, and C. L. Degen, Annu. Rev. Phys. Chem. **65**, 83 (2014).
[46] C. Li, M. Chen, D. Lyzwa, and P. Cappellaro, Nano Lett. **19**, 7342 (2019).
[47] S. Schmitt, T. Gefen, F. M. Stürner, T. Unden, G. Wolff, C. Müller, J. Scheuer, B. Naydenov, M. Markham,

S. Pezzagna, J. Meijer, I. Schwarz, M. Plenio, A. Retzker, L. P. McGuinness, and F. Jelezko, Science **356**, 832 (2017).

[48] G. Wang, Y.-X. Liu, Y. Zhu, and P. Cappellaro, Nano Lett. **21**, 5143 (2021).

[49] J.-C. Jaskula, K. Saha, A. Ajoy, D. J. Twitchen, M. Markham, and P. Cappellaro, Phys. Rev. Applied **11**, 054010 (2019).

[50] Here we did not choose amplitude-modulated CCD, since it is still limited by the total microwave power and amplifier nonlinearity [23].

[51] B. R. Mollow, Phys. Rev. **188**, 1969 (1969).

[52] B. Pigeau, S. Rohr, L. Mercier de Lépinay, A. Gloppe, V. Jacques, and O. Arcizet, Nat. Commun. **6**, 8603 (2015).

[53] The particle-hole symmetry operator $\hat{P}_1$ here maps one eigenstate to its counterpart such that $\mu' = \mp$ corresponding to $\mu = \pm$.

[54] E. R. MacQuarrie, T. A. Gosavi, A. M. Moehle, N. R. Jungwirth, S. A. Bhave, and G. D. Fuchs, Optica **2**, 233 (2015).

[55] E. R. MacQuarrie, T. A. Gosavi, N. R. Jungwirth, S. A. Bhave, and G. D. Fuchs, Phys. Rev. Lett. **111**, 227602 (2013).

[56] J. Tindall, C. S. Muñoz, B. Buča, and D. Jaksch, New J. Phys. **22**, 013026 (2020).

[57] O. E. Alon, Phys. Rev. A **66**, 013414 (2002).

[58] O. E. Alon, V. Averbukh, and N. Moiseyev, Phys. Rev. Lett. **85**, 5218 (2000).

[59] O. E. Alon, V. Averbukh, and N. Moiseyev, Phys. Rev. Lett. **80**, 3743 (1998).